The Role of Slow Potassium Current in Nerve Conduction Block Induced by High-Frequency Biphasic Electrical Current

Hailong Liu, James R. Roppolo, William C. de Groat, and Changfeng Tai*, *Senior Member, IEEE*

***Abstract*—The role of slow potassium current in nerve conduction block induced by high-frequency biphasic electrical current was analyzed using a lumped circuit model of a myelinated axon based on the Schwarz–Reid–Bostock model. The results indicate that nerve conduction block at stimulation frequencies above 4 kHz is due to constant activation of both fast and slow potassium channels, but the block at stimulation frequencies below 4 kHz could be due to either anodal or cathodal dc block depending on the time of the action potiential arriving at the block electrode. When stimulation frequency was above 4 kHz, the slow potassium current was about 3.5 to 6.5 times greater than the fast potassium current at blocking threshold, indicating that the slow potassium current played a more dominant role than the fast potassium current. The blocking location moved from the node under the blocking electrode to a nearby node as the stimulation intensity increased. This simulation study reveals that in mammalian myelinated axons, the slow potassium current probably plays a critical role in the nerve conduction block induced by high-frequency biphasic electrical current.**

***Index Terms*—Axon, block, high frequency, potassium, stimulation.**

I. Introduction

REVERSIBLE nerve conduction block induced by high-frequency biphasic electrical current has many potential clinical applications, for example, alleviating chronic pain [1], stopping unwanted muscle movements (muscle spasms and spasticity) [2], and improving voiding efficiency [3]. Since high-frequency biphasic electrical stimulation causes less tissue damage than uniphasic stimulation due to electrochemical reactions [4], it is a very promising approach for long-term clinical application. Although many experiments [2], [3], [5]–[12] have been performed recently to investigate this type of nerve conduction block, the underlying mechanisms are still uncertain.

It has been known for more than 60 years that high-frequency biphasic electrical current could block nerve conduction [8], [9]. However, due to the electrical noise induced by the high-frequency blocking stimulation, it is very difficult to investigate the blocking mechanisms in animal experiments using traditional electrophysiological methods. Therefore, recent studies [2], [12]–[18] have focused on computer simulation using axonal models. Our previous studies [14]–[18] using both amphibian and mammalian axon models indicated that the fast potassium current might play a role in nerve conduction block induced by high-frequency biphasic electrical current. However, there is a significant difference in nodal potassium current between mammalian and amphibian axons. The node of amphibian (frog) myelinated axons has a large fast potassium current [19], whereas in mammalian myelinated axons, the slow potassium current is significantly larger than the fast potassium current [20], [21]. The role of slow potassium channels in the conduction block of mammalian myelinated axons has not been investigated.

This study used the Schwarz–Reid–Bostock (SRB) axonal membrane model, which was derived from human axonal data and incorporates both fast and slow potassium channels. The goal of this study was to further examine the mechanisms underlying nerve conduction block induced in mammalian myelinated axons by high-frequency biphasic electrical current with a particular focus on the possible role of slow potassium current.

II. Methods

The nerve model used in this study is shown in Fig. 1. A 60-mm-long myelinated axon is modeled with an internode length $\Delta x = 100d$ (where d is the axon diameter) and $d = 0.7D$ (where D denotes the axon external myelin diameter). The nodal length is denoted by L. Each node of the axon is modeled by a membrane capacitance (C_m) and a variable membrane resistance (R_m). R_a is the internode axoplasm resistance. The ionic currents passing through the variable membrane resistance are described by the SRB model (see the Appendix and [22]). Two monopolar point electrodes (with the indifferent electrode at infinity) are placed at 1 mm distance to the axon (see Fig. 1). One is the block electrode at the 30 mm location along the axon, where the high-frequency biphasic rectangular pulses are delivered (as shown in Fig. 1). The other is the test electrode at the 10 mm location, which delivers a uniphasic single pulse (pulsewidth 0.1 ms and intensity 3 mA) to evoke an action potential and test whether this action potential can propagate through the site of the block electrode. The test electrode is always a cathode (negative pulse), and the block electrode always delivers biphasic square pulses with the cathodal phase first (see Fig. 1).

Manuscript received March 21, 2008; revised July 8, 2008. First published October 3, 2008; current version published February 13, 2009. This work was supported by the National Institutes of Health (NIH) under Grant RO1-DK-068566 and Grant RO1-NS-051671. *Asterisk indicates corresponding author.*

H. Liu is with the Department of Urology and the Department of Pharmacology, University of Pittsburgh, Pittsburgh, PA 15261 USA.

J. R. Roppolo and W. C. de Groat are with the Department of Pharmacology, University of Pittsburgh, Pittsburgh, PA 15261 USA.

*C. Tai is with the Department of Urology, University of Pittsburgh, Pittsburgh, PA 15261 USA (e-mail: cftai@pitt.edu).

Digital Object Identifier 10.1109/TBME.2008.2006013

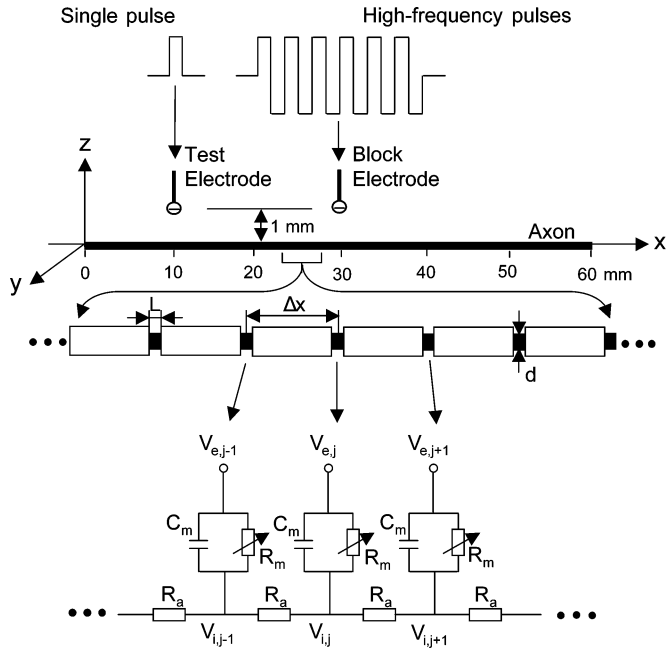

Fig. 1. Myelinated axonal model used to simulate conduction block induced by high-frequency biphasic electrical current. The internode length $\Delta x = 100d$; d is the axon diameter. L is the nodal length. Each node is modeled by a resistance–capacitance circuit based on the SRB model. R_a: internodal axoplasmic resistance; R_m: nodal membrane resistance; C_m: nodal membrane capacitance; $V_{i,j}$: intracellular potential at the jth node; $V_{e,j}$: extracellular potential at the jth node.

We assume that the axon is in an infinite homogeneous medium (extracellular resistivity $\rho_e = 0.3$ kΩ·cm). After neglecting the small influence induced by the presence of the axon in the homogeneous medium, the extracellular potential $V_{e,j}$ at the jth node along the axon can be calculated by

$$V_{e,j}(t) = \frac{\rho_e}{4\pi}\left[\frac{I_{\text{block}}(t)}{\sqrt{(j\Delta x - x_0)^2 + z_0^2}} + \frac{I_{\text{test}}(t)}{\sqrt{(j\Delta x - x_1)^2 + z_1^2}}\right]$$

where $I_{\text{block}}(t)$ is the high-frequency biphasic pulse current delivered to the block electrode (at location $x_0 = 30$ mm, $z_0 = 1$ mm), and $I_{\text{test}}(t)$ is the single test pulse delivered to the test electrode (at location $x_1 = 10$ mm, $z_1 = 1$ mm).

The change of the membrane potential V_j at the jth node is described by

$$\frac{dV_j}{dt} = \frac{1}{c_m}\left[\frac{d}{4\rho_i L\Delta x}(V_{j-1} - 2V_j + V_{j+1} + V_{e,j-1} - 2V_{e,j} + V_{e,j+1}) - i_{i,j}\right]$$

where $V_j = V_{i,j} - V_{e,j} - V_{\text{rest}}$; $V_{i,j}$ is the intracellular potential at the jth node; $V_{e,j}$ is the extracellular potential at the jth node; V_{rest} is the resting membrane potential; c_m is the membrane capacitance per unit area; ρ_i is the intracellular axoplasm resistivity; $i_{i,j}$ is the ionic current density at the jth node described by SRB equations (see the Appendix and [22]).

The SRB model was derived from the total nodal current instead of current density. In order to normalize the model, the axon diameter used to develop the SRB model needs to be estimated, which was not given in the original SRB model [22]. It is known that the relationships between axonal diameter and the duration and conduction velocity of action potential are affected by temperature [23]. The duration of action potential recorded at 25 °C is 1.4 ms in the SRB model [22]. According to Paintal's experimental data [23], the conduction velocity v could be estimated to be 64 m/s in the SRB model. Based on $v = D \times 5.7 \times 10^6$ given by Boyd and Kalu [24], the estimated axon external myelin diameter D is 11.23 μm in the SRB model. Therefore, the axon diameter $d = 0.7D = 7.86$ μm was used in this study to convert the parameters in the original SRB model to the values per unit area (see Table I).

TABLE I
PARAMETERS USED IN THE SRB MODEL

Symbol	Description	Value
V_{rest} (mV)	resting membrane potential	-84
E_{K} (mV)	potassium equilibrium potential	-84
E_{L} (mV)	unspecific ion equilibrium potential	-84
g_{Kf} (mS/cm^2)	fast potassium conductance per unit area	60.75
g_{Ks} (mS/cm^2)	slow potassium conductance per unit area	121.51
g_{L} (mS/cm^2)	leakage conductance per unit area	121.51
c_{m} (μF/cm^2)	membrane capacitance per unit area	5.67
P_{Na} (cm/s)	sodium permeability	0.01426
$[\text{Na}]_{\text{o}}$ (mmole/l)	extracellular sodium concentration	154
$[\text{Na}]_{\text{i}}$ (mmole/l)	intracellular sodium concentration	35
L (cm)	nodal length	1.0*10^{-4}
F (C/mole)	Faraday constant	96485
R (mJ/K/mole)	gas constant	8314.4
ρ_{e} (kΩ•cm)	extracellular resistivity	0.3
ρ_{i} (kΩ•cm)	intracellular resistivity	0.11
T (Kelvin)	temperature	310.15

The axonal model was solved by the Runge–Kutta method [25] with a time step of 0.001 ms. The simulation was always performed with the initial condition $V_j = 0$ and the temperature $T = 37$ °C. The membrane potentials at the two end nodes of the modeled axon were always equal to the membrane potentials of their closest neighbors, which implemented sealed boundary conditions (no longitudinal currents) at the two ends of the modeled axon.

III. RESULTS

A. Nerve Conduction Block Induced by High-Frequency Biphasic Electrical Current

The SRB model successfully simulated the conduction block induced by high-frequency biphasic electrical current. As an example, Fig. 2 shows a typical nerve firing pattern and conduction block at different stimulation intensities. The locations of the test and block electrodes are marked by short arrows along the axon [see Fig. 2(a)]. The single test pulse and the high-frequency biphasic blocking pulses are schematically plotted

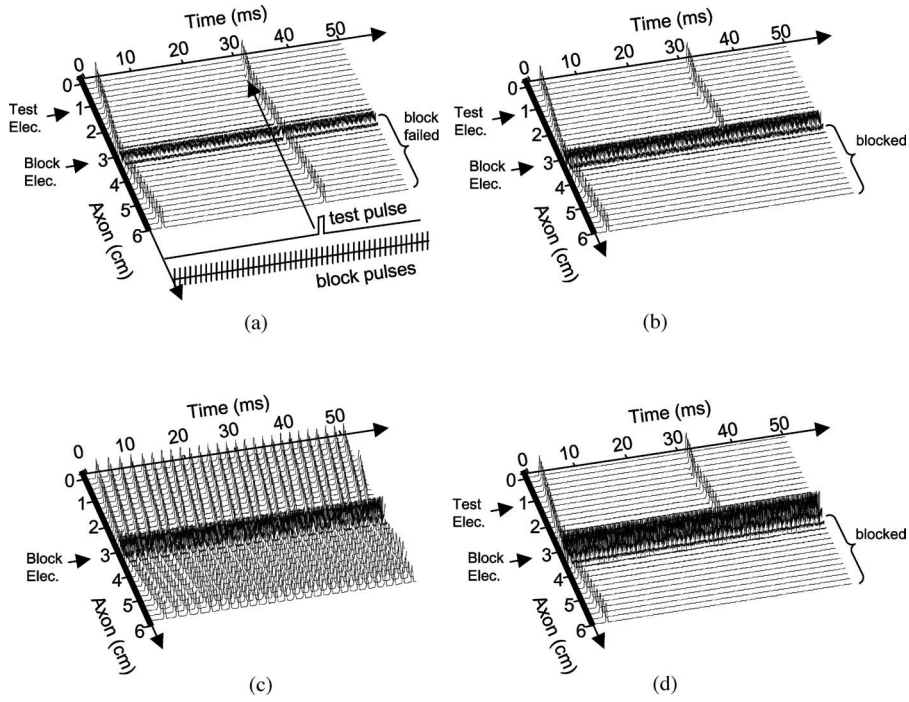

Fig. 2. Propagation of action potentials along an axon induced by high-frequency biphasic stimulation at different intensities. The short arrows mark the locations of test and block electrodes along the axon in each figure. Axon diameter: 5 μm. Stimulation: 7 kHz. (a) 1.8 mA. (b) 3.0 mA. (c) 5.2 mA. (d) 8.0 mA.

on the side in Fig. 2(a) to show the timing of the two different stimulations. With the stimulation intensity below the block threshold as shown in Fig. 2(a), the high-frequency blocking stimulation generated an initial action potential (at location 3 cm) that propagated in two directions. Then, the high-frequency stimulation alternatively depolarized and hyperpolarized the axon membrane without generating any action potential. At the time 30 ms, an action potential was initiated by the test electrode (at location 1 cm), and it propagated through the site of the block electrode (at location 3 cm). When the intensity of high-frequency stimulation was increased above the block threshold, as shown in Fig. 2(b), the propagation of action potential evoked by the test electrode was blocked. However, further increasing the intensity of high-frequency stimulation caused repetitive firing, as shown in Fig. 2(c), although the high-frequency stimulation induced only an initial action potential at other intensities [see Fig. 2(a), (b), and (d)]. This repetitive firing disappeared, and nerve conduction could be blocked again if the stimulation intensity increased further [see Fig. 2(d)].

Fig. 3 shows the pattern of nerve conduction block and repetitive firing at different stimulation frequencies (1–10 kHz) and intensities (0–10 mA) for axons of different diameters (2, 5, 10, and 20 μm). At low frequencies (<4 kHz), the axon could fire repetitively over a large range of stimulation intensities, and nerve block only occurred in a narrow range of stimulation intensities. However, when the frequency was increased above 4 kHz, the nerve conduction could be blocked over a large range of stimulation intensities. The blocking threshold became lower as the axonal diameter increased.

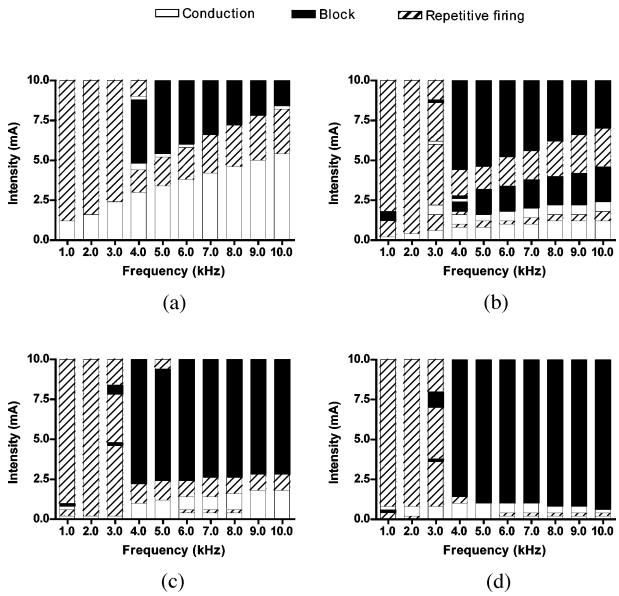

Fig. 3. Pattern of nerve block and repetitive firing at different stimulation frequencies and intensities for axons of different diameters. The black areas represent the stimulation intensity ranges causing nerve block, as shown in Fig. 2(b) or (d). The hatched areas represent repetitive firing, as shown in Fig. 2(c). The white areas represent nerve conduction block failure, as shown in Fig. 2(a). (a) 2 μm. (b) 5 μm. (c) 10 μm. (d) 20 μm.

B. Mechanism of Nerve Conduction Block

Three different blocking mechanisms were identified. At stimulation frequencies below 4 kHz, anodal or cathodal block occurred. However, at stimulation frequencies above 4 kHz, the

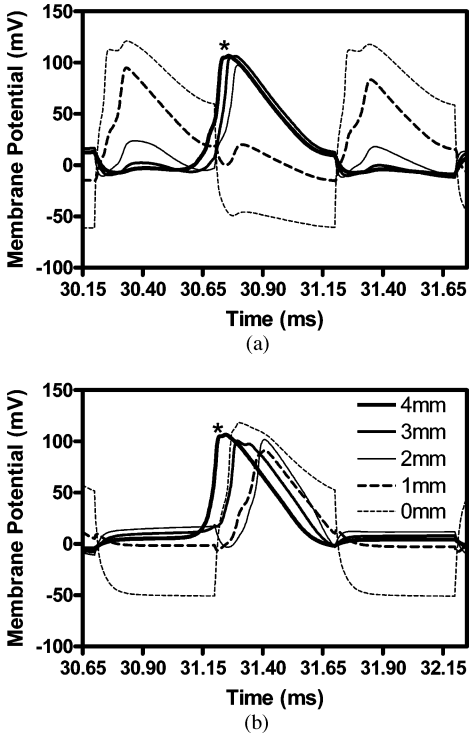

Fig. 4. Propagation of membrane potentials near the block electrode when (a) anodal or (b) cathodal block occurs. The legend in (b) indicates the distance from the block electrode for both (a) and (b). The thinnest dashed line (0 mm) corresponds to the node under the block electrode (i.e., at 30 mm location). The thickest solid line (4 mm) corresponds to the node 4 mm away from the block electrode (i.e., at 26 mm location). The anodal block (a) occurred at 1-mA stimulation intensity for a 10-μm axon. The cathodal block (b) occurred at 1.6-mA stimulation intensity for a 5-μm axon. Stimulation frequency: 1 kHz. The asterisks mark the propagating action potential from the test electrode.

constant activation of potassium channels played a critical role in the nerve conduction block.

Fig. 4 shows that an anodal or a cathodal block occurred at a stimulation frequency of 1 kHz. The legend in Fig. 4(b) indicates the distance of each node from the block electrode. The node at 0 mm was under the block electrode. As shown in Fig. 4(a), the propagating action potential initiated by the test electrode arrived at the block electrode when the biphasic blocking current was in the anodal phase. The propagating action potential from the test electrode was marked by a "$*$." The strong hyperpolarization induced by the anodal pulse under the blocking electrode caused the conduction failure of the action potential. In Fig. 4(b), the propagating action potential arrived at the block electrode when the biphasic blocking current was in the cathodal phase. The strong depolarization at the block electrode induced by the cathodal pulse caused the conduction block of the action potential.

At stimulation frequencies above 4 kHz, a completely different blocking mechanism was identified. Fig. 5(a) shows the nerve conduction block at a stimulation frequency of 7 kHz. The black frame in Fig. 5(a) circled the area where nerve block occurred, which included the data from nine consecutive nodes at distances 0–4 mm away from the block electrode. The area is enlarged and redrawn in Fig. 5(b) to show the details. The activity of the nearest five nodes to the block electrode are shown in Fig. 5(c)–(j). The propagation of the action potential as well as the sodium and potassium currents associated with the action potential were completely abolished at the node (0 mm) under the blocking electrode where axonal membrane was alternatively depolarized and hyperpolarized [see Fig. 5(c)–(f)]. As the action potential propagated toward the blocking electrode, the activation (m) of sodium channels became oscillatory at the node under the blocking electrode [see Fig. 5(g)] while the inactivation (h) remained at a relatively constant level [see Fig. 5(h)], resulting in a pulsed inward sodium current [see Fig. 5(d)]. Therefore, the sodium channels were never completely blocked when conduction block occurred. The activation of both fast (n) and slow (s) potassium channels became constant at the node under the block electrode [see Fig. 5(i) and (j)] resulting in large pulsed outward fast and slow potassium currents [see Fig. 5(e) and (f)]. The large outward potassium currents opposed the large inward sodium current, which caused the node under the block electrode to become unexcitable leading to the block of nerve conduction. Therefore, the mechanism of conduction block at frequencies above 4 kHz was due to the activation of both fast and slow potassium channels under the blocking electrode. However, note that the maximal slow potassium current was much larger (about 3.5 times) than the fast potassium current at the node under the block electrode [see Fig. 5(e) and (f)], which indicated that slow potassium current might be more critical than fast potassium current in blocking nerve conduction. For the purpose of discussion in this paper, this blocking mechanism is termed as "potassium block."

The "potassium block" could occur not only at the node under the block electrode but also at nodes adjacent to the block electrode as the stimulation intensity increased. As shown in Fig. 6, at a low stimulation intensity (2.2 mA), the conduction block occurred at the node under the block electrode at the 30 mm location [see Fig. 6(a)], but at a high stimulation intensity (8 mA), the conduction block occurred at the node 2 mm away from the block electrode [i.e., at the 28 mm location, see Fig. 6(b)]. This is due to the fact that at 8-mA current intensity, the range of membrane potential oscillations at the 28 mm location was approximately equivalent to that at the 30 mm location when stimulation intensity was 2.2 mA. The activating function ($\Delta^2 V_{e,j}/\Delta x^2$) [26], [27] during the anodal or cathodal phase of the high-frequency blocking stimulation was also plotted in Fig. 6 for stimulation intensities of 2.2 and 8 mA, respectively. A positive value of the activating function depolarizes the axonal membrane, whereas a negtive value hyperpolarizes the membrane [26], [27]. It can be seen that the range between the anodal and cathodal activating functions at the 28 mm location (i.e., the "side lobe") when stimulation intensity is 8 mA [see Fig. 6(b)] is about the same as the range at the 30 mm location when stimulation intensity is 2.2 mA [see Fig. 6(a)]. This causes the node at the 28 mm location to be alternatively depolarized and hyperpolarized by the 8-mA stimulation to the same extent as the node at the 30 mm location during 2.2-mA stimulation. The "side lobe" of the activating function explains

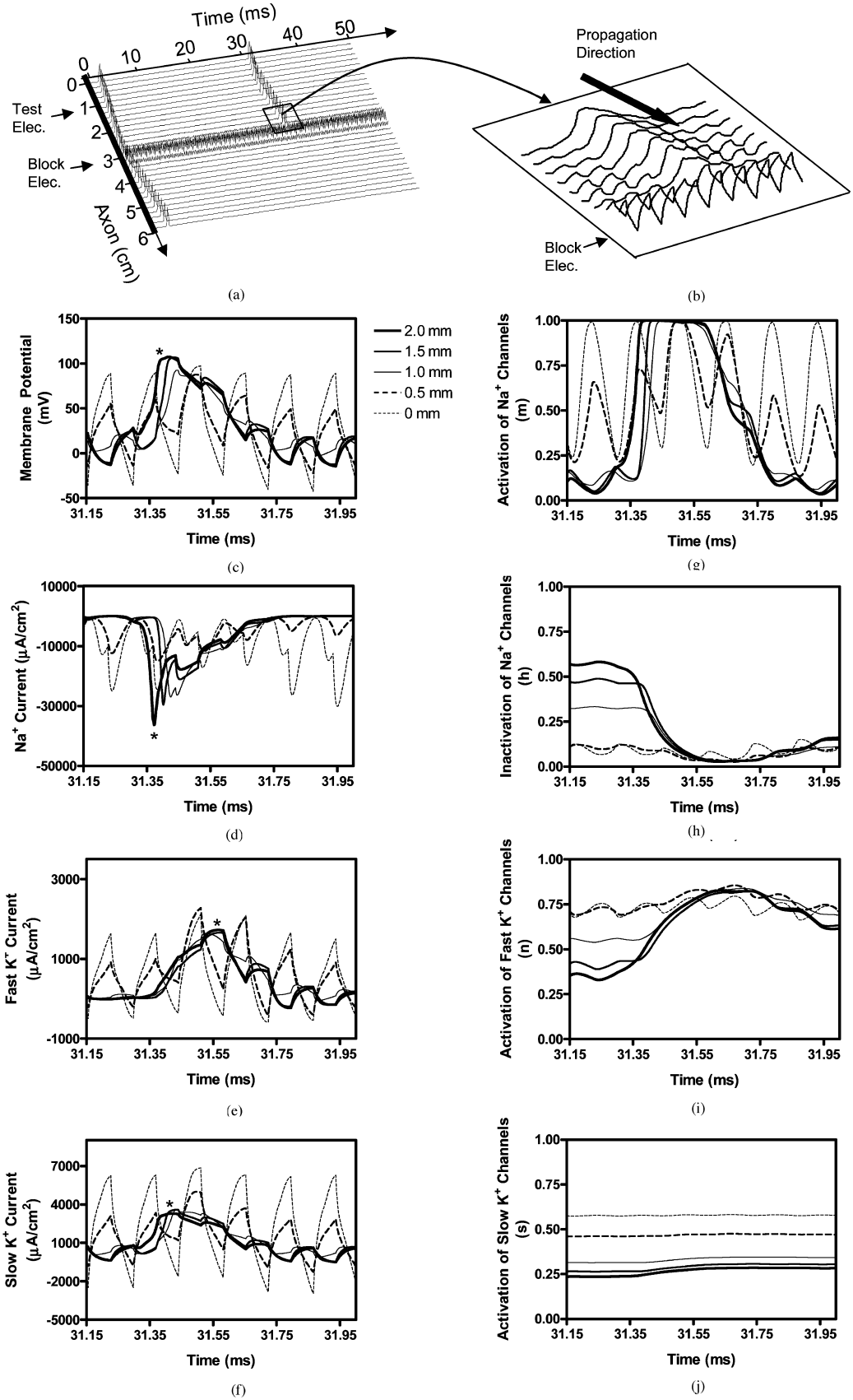

Fig. 5. Propagation of membrane potential, ionic current, and activation/inactivation of ion channels near the block electrode when potassium block occurs. The legend in (c) indicates the distance from the block electrode (0 mm is under the block electrode). The propagation of membrane potential near the block electrode is shown in detail in (b). Stimulation: intensity 2.2 mA, frequency 7 kHz. Axon diameter: 5 μm. The asterisks in (c)–(f) mark the propagating action potential from the test electrode, and its corresponding ionic currents.

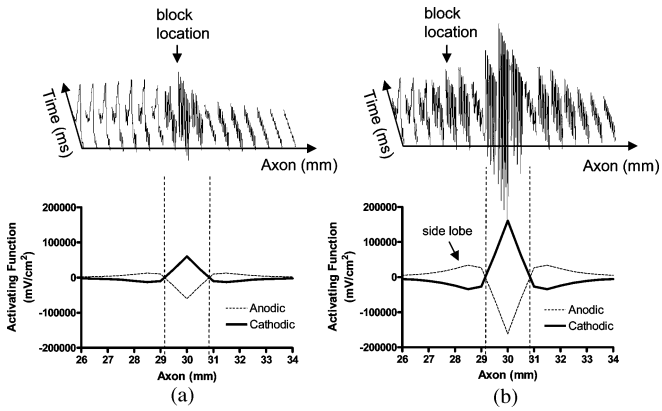

Fig. 6. Block locations and activating functions at (a) 2.2 mA and (b) 8 mA stimulation intensities. The upper trace showing the membrane potentials at different nodes shares the same horizontal axis as the lower trace showing the activating functions. The block electrode is located at 30 mm. The activating functions for both anodal and cathodal pulses are shown. (a) Nerve conduction was blocked at the node under the block electrode. (b) Block occurred at the node 2 mm away (at 28 mm) from the block electrode. Stimulation frequency: 7 kHz. Axon diameter: 5 μm.

why at a high stimulation intensity the block location moves to the node adjacent to the block electrode.

C. Role of Slow Potassium Current

Fig. 7(a)–(d) shows that at different frequencies and intensities, the maximal activation of fast potassium channels is almost the same [see Fig. 7(a) and (b)], whereas the activation of slow potassium channels is increased as the frequency decreases [see Fig. 7(c)] or as the intensity increases [see Fig. 7(d)]. The conduction block occurs only when the activation of slow potassium channels is above 0.56 [see Fig. 7(c) and (d)]. Fig. 8 is similar to Fig. 7 except that the axonal diameter is 20 μm instead of 5 μm. Again, the activation of fast potassium channels has almost the same maximal values for different frequencies [see Fig. 8(a)] or intensities [see Fig. 8(b)], but the activation of slow potassium channels is increased as the intensity increases [see Fig. 8(d)]. However, the activation of slow potassium channels in the 20 μm axon is increased as the frequency increases [see Fig. 8(c)], which is different from the 5-μm axon [see Fig. 7(c)]. This difference is consistent with the decrease of the blocking threshold as the frequency increases, as shown in Fig. 3(d) for a 20 μm axon, whereas the blocking threshold increases as the frequency increases, as shown in Fig. 3(b) for a 5 μm axon. The fact that the slow potassium channels have to be activated above a certain level to induce a block [see Figs. 7(c) and (d) and 8(c) and (d)] indicates that the slow potassium channels may play a critical role in nerve conduction block. This is further supported by the observation that at different blocking thresholds, the activation of slow potassium channels remains in a relatively narrow range although the frequency and intensity are very different [see Fig. 9(a)], while the inactivation of sodium channels is oscillating around 0.1 and can be further inactivated when action potential arrives [see Fig. 9(b)].

Based on the SRB model (see the Appendix and [22]), the ratio between slow and fast potassium currents is $i_{Ks}/i_{Kf} = 2s/n^4$. Further quantitative analysis of fast and slow potassium currents shows that at blocking thresholds, the activation of fast potassium channels (n) has a range of about 0.65–0.75, and the activation of slow potassium channels (s) has a range of about 0.55–0.57 for a 5-μm axon. Therefore, it can be estimated that the ratio ($2s/n^4$) between slow and fast potassium currents is about 3.5–6.5 at blocking thresholds (see Fig. 10). This indicates a dominant role of the slow potassium current over the fast potassium current in nerve conduction block.

IV. Discussion

This simulation study employing a mammalian myelinated axonal model based on SRB equations investigated the nerve conduction block induced by high-frequency biphasic electrical current. Several possible mechanisms underlying nerve block were identified including anodal block [see Fig. 4(a)], cathodal block [see Fig. 4(b)], and potassium block (see Fig. 5). At stimulation frequencies below 4 kHz, anodal or cathodal block occurred due to membrane hyperpolarization or depolarization, but at stimulation frequencies above 4 kHz, the constant activation of both slow and fast potassium channels played a critical role in blocking nerve conduction. When stimulation frequency is above 4 kHz, more slow potassium current (about 3.5–6.5 times the fast potassium current) was induced at blocking thresholds, indicating that in mammalian myelinated axons, the slow potassium current played a more prominent role in nerve conduction block than the fast potassium current.

The block location moved from the node under the block electrode to a nearby node as stimulation intensity increased due to the "side lobe" effect of the activating function [see Fig. 6(b)]. The blocking stimulation also induced repetitive firing of action potentials at the "side lobe" region at stimulation intensities above the blocking threshold for stimulation frequencies from 4 to 10 kHz in a 5-μm axon, as shown in Fig. 3(b). This "side lobe" induced firing divided the blocking intensity range into two parts [see Fig. 3(b)]. The lower intensity range produced nerve block under the blocking electrode, but the higher intensity range blocked nerve conduction at the "side lobe" region close to the blocking electrode. The "side lobe" induced firing was not seen to divide the blocking intensity range in other axons of different diameters [see Fig. 3(a), (c), and (d)]. This indicates that in a compound nerve consisting of many axons of different diameters, the blocking stimulation might block the majority of axon fibers, but cause a small percent of axons to fire repetitively. Only a monopolar blocking electrode is investigated in this study. Different geometry of the blocking electrode (monopolar, bipolar, or tripolar) will produce a significantly different shape of the activating function [26], [27]. This may result in a "side lobe" effect that is very different from what is shown in Fig. 6. Therefore, the geometry of the blocking electrode needs to be considered when applying high-frequency biphasic stimulation to block nerve conduction. It is also worth noting that the blocking electrode is positioned on top of the axonal node at a fixed distance (1 mm), and the electrical properties of the internodal region are neglected in this study. Changing the electrode position or incoporating the internodal region into

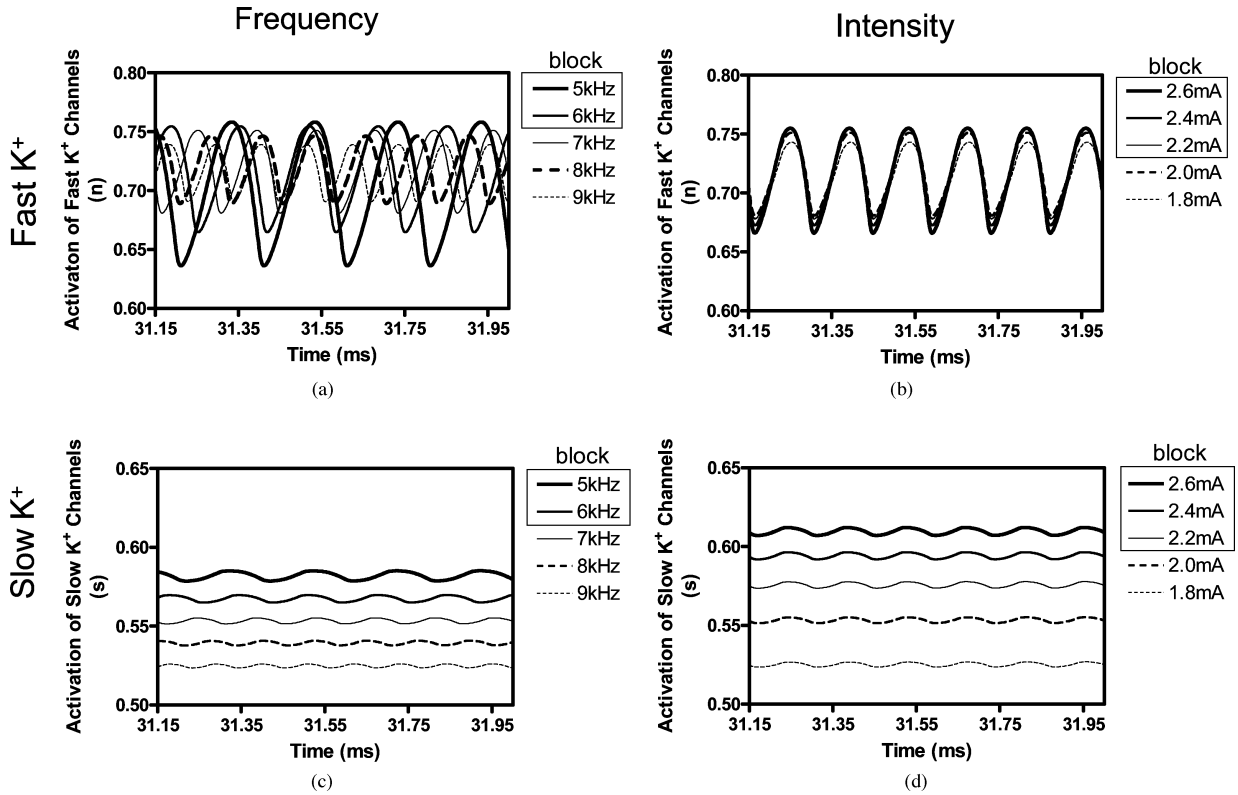

Fig. 7. Activation of fast [n in (a) and (b)] and slow [s in (c) and (d)] potassium channels at different stimulation frequencies [(a) and (c)] and intensities [(b) and (d)] for the node under the block electrode. In (a) and (c), the stimulation intensity is 2 mA. In (b) and (d), the stimulation frequency is 7 kHz. The parameters in the legend enclosed by a square box are above the blocking threshold. Axon diameter: 5 μm.

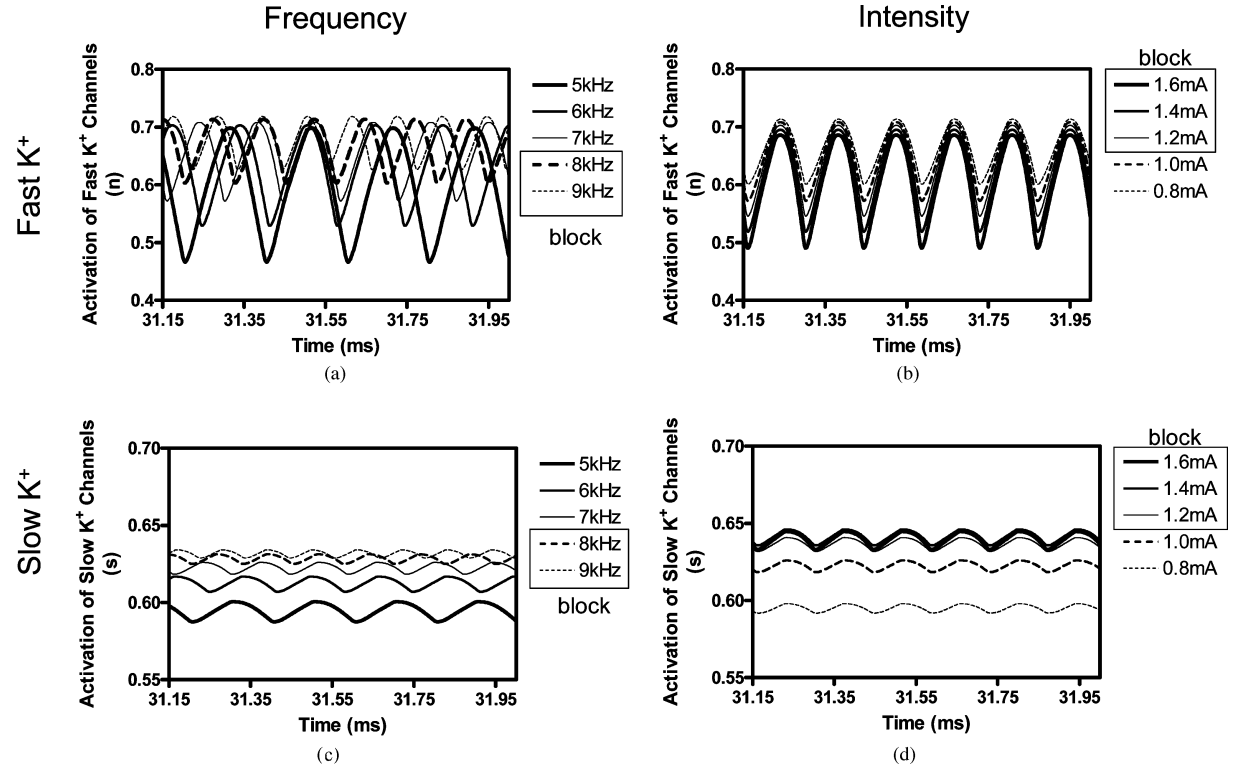

Fig. 8. Activation of fast [n in (a) and (b)] and slow [s in (c) and (d)] potassium channels at different stimulation frequencies [(a) and (c)] and intensities [(b) and (d)] for the node under the block electrode. In (a) and (c), the stimulation intensity is 1 mA. In (b) and (d), the stimulation frequency is 7 kHz. The parameters in the legend enclosed by a square box are above the blocking threshold. Axon diameter: 20 μm.

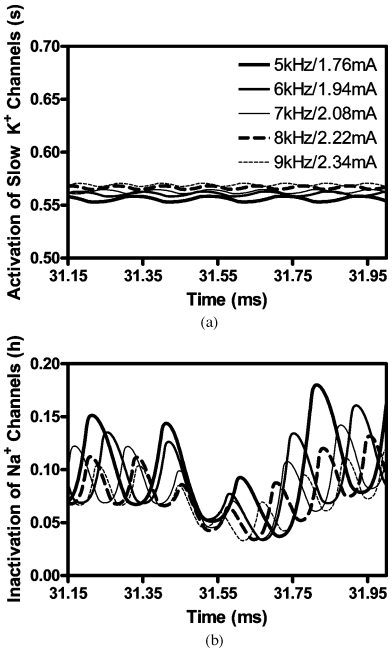

Fig. 9. (a) Activation of slow potassium channels and (b) inactivation of sodium channels at the node under the block electrode for different blocking thresholds. The legend in (a) shows the intensity thresholds at different frequencies. Axon diameter: 5 μm.

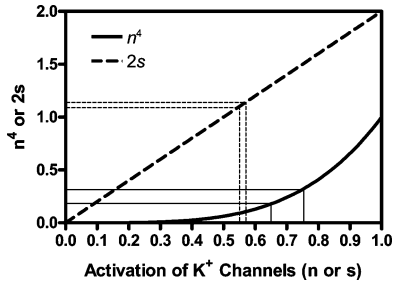

Fig. 10. Contribution of fast (n) and slow (s) potassium currents to nerve conduction block at the blocking threshold level. The single solid line represents n^4. The double solid lines indicate the range of fast potassium activation at blocking thresholds and the corresponding range for n^4. The single dashed line represents $2s$. The double dashed lines indicate the range of slow potassium activation at blocking thresholds and the corresponding range for $2s$. At blocking thresholds, $2s/n^4$ is about 3.5–6.5 indicating that slow potassium current is more dominant than fast potassium current. Axon diameter: 5 μm.

the model could influence the blocking thresholds resulting in a shift of the blocking intensity range in Fig. 3. However, the minimal blocking frequency shown in Fig. 3 and the blocking mechanisms identified in Figs. 4 and 5 should remain the same. Since a small time step of 0.001 ms was used in this simulation study, the numerical error of the calculated blocking threshold was estimated to be less than 0.1 mA.

The node of amphibian (frog) myelinated axons has mainly a fast potassium current [19], whereas mammalian myelinated axons have both fast and slow potassium currents, and the slow potassium current is dominant over the fast potassium current [20], [21]. Our previous simulation studies [16], [17] using the Frankenhaeuser–Huxley model [19] based on amphibian axons showed that the fast potassium current played a critical role in nerve conduction block. However, this study using a mammalian myelinated axonal model showed that the slow potassium current had a more important role than the fast potassium current. Although previous studies [2], [3], [5]–[12] in cats, rats, and frogs all reported nerve conduction block at stimulation frequencies above 4 kHz, the underlying mechanisms may be very different for amphibian and mammalian.

The results obtained in this study need to be further confirmed by both animal studies and simulation analysis. Simulation analysis with other axonal models may further verify the role of slow potassium currents in nerve conduction block. The McIntyre–Richardson–Grill (MRG) model [28] also incorporates slow and fast potassium currents. However, a previous study [13] employing the MRG model did not investigate the role of slow potassium current in nerve conduction block. Therefore, a simulation study based on the MRG model should be performed to further verify the role of slow potassium channels. It is worth noting that this study used a McNeal-type axonal model that did not incorporate a detailed representation of the internodal region. However, this study and previous studies using McNeal-type models [16]–[18] have sucessfully simulated the nerve conduction block phenomena observed in animal studies [2], [3], [5]–[11]. They also produced very similar results as the study [13] using the MRG model that incorporated a detailed representation of the internodal region, indicating that the internodal region might not be involved in the possible mechanisms underlying the nerve conduction block induced by high-frequency biphasic electrical stimulation. Simulation studies using more complex axon models [29]–[31] that incorporate more realistic extracellular space, glial buffering, and ion pumps may further reveal the role of potassium channels in nerve conduction block.

Previous studies [32]–[34] in rat hippocampal slices showed that the neuronal epileptiform activity and axonal conduction could be blocked by high-frequency (<500 Hz) sinusoidal electrical field stimulation. The block was always coincident with a stimulus-induced rise in extracelluar potassium concentration, suggesting the opening of the potassium channels and potassium outflow from the neurons/axons during the stimulation. The stimulation frequency to block the hippocampal neuron/axon is relatively low (<500 Hz) compared to the minimal stimulation frequency required to block the conduction of peripheral nerve (1–10 kHz) [2], [3], [5]–[12]. However, this frequency discrepancy might be caused by the slow membrane dynamics of the hippocampal neuron/axon. The duration of the action potential generated in neurons can be several milliseconds long [35], but it is less than 1 ms in mammalian myelinated axons of the peripheral nervous system. Our previous simulation study [18] has shown that a lower stimulation frequency is required to block the nerve when the membrane dynamics become slower. Whether the slow potassium channels also play an important role in blocking the hippocampal neuron/axon needs to be further investigated.

A reversible nerve conduction block method will find many applications in both clinical medicine and basic neuroscience [1]–[11]. Understanding the biophysics and mechanisms underlying the nerve conduction block induced by high-frequency biphasic electrical current could promote its clinical application

and possibly the design of new stimulation waveforms using less current to block nerve conduction. Simulation analysis using computer models provides a tool to reveal mechanisms underlying the nerve conduction block and may help to design new animal experiments to further test new nerve blocking methods.

APPENDIX: SRB MODEL

The ionic current density $i_{i,j}$ at the jth node is described as

$$\begin{aligned} i_{i,j} &= i_{\mathrm{Na}} + i_{Kf} + i_{Ks} + i_L \\ i_{\mathrm{Na}} &= m^3 h P_{\mathrm{Na}} \frac{EF^2}{RT} \frac{[\mathrm{Na}]_o - [\mathrm{Na}]_i \exp(EF/RT)}{1-\exp(EF/RT)} \\ i_{Kf} &= n^4 g_{Kf}(E-E_K) \\ i_{Ks} &= s g_{Ks}(E-E_K) \\ i_L &= g_L(E-E_L). \end{aligned}$$

The evolution equations for variables $m,\ h,\ n$, and s are

$$\begin{aligned} dm/dt &= [\alpha_m(1-m) - \beta_m m]\, k_m \\ dh/dt &= [\alpha_h(1-h) - \beta_h h]\, k_h \\ dn/dt &= [\alpha_n(1-n) - \beta_n n]\, k_n \\ ds/dt &= [\alpha_s(1-s) - \beta_s s]\, k_s \end{aligned}$$

where

$$\begin{aligned} \alpha_m &= \frac{1.86(E+18.4)}{1-\exp[(-18.4-E)/10.3]} \\ \alpha_n &= \frac{0.00798(E+93.2)}{1-\exp[(-93.2-E)/1.1]} \\ \beta_m &= \frac{0.086(-22.7-E)}{1-\exp[(E+22.7)/9.16]} \\ \beta_n &= \frac{0.0142(-76.0-E)}{1-\exp[(E+76.0)/10.5]} \\ \alpha_h &= \frac{0.0336(-111.0-E)}{1-\exp[(E+111.0)/11.0]} \\ \alpha_s &= \frac{0.00122(E+12.5)}{1-\exp[(-12.5-E)/23.6]} \\ \beta_h &= \frac{2.30}{1+\exp[(-28.8-E)/13.4]} \\ \beta_s &= \frac{0.000739(-80.1-E)}{1-\exp[(E+80.1)/21.8]} \end{aligned}$$

and

$$\begin{aligned} k_m &= 2.2^{(T-293.15)/10} \\ k_h &= 2.9^{(T-293.15)/10} \\ k_n &= 3.0^{(T-293.15)/10} \\ k_s &= 3.0^{(T-293.15)/10} \end{aligned}$$

where T is the temperature (310.15 °K, i.e., 37 °C) and $E = V_j + V_{\mathrm{rest}}$. The initial values for $m,\ h,\ n$, and s are 0.0382, 0.6986, 0.2563, and 0.2011, respectively, which correspond to the initial condition $V_j = 0$, or $E = V_{\mathrm{rest}} = -84$ mV.

REFERENCES

[1] B. Nashold, J. Goldner, J. Mullen, and D. Bright, "Long-term pain control by direct peripheral-nerve stimulation," *J. Bone Joint Surg.*, vol. 64, no. 1, pp. 1–10, 1982.

[2] K. Kilgore and N. Bhadra, "Nerve conduction block utilising high-frequency alternating current," *Med. Biol. Eng. Comput.*, vol. 42, no. 3, pp. 394–406, May 2004.

[3] C. Tai, J. Roppolo, and W. de Groat, "Block of external urethral sphincter contraction by high frequency electrical stimulation of pudendal nerve," *J. Urol.*, vol. 172, no. 5, pp. 2069–2072, 2004.

[4] W. Agnew and D. McCreery Eds., *Neural Prostheses: Fundamental Studies*. Englewood Cliffs, NJ: Prentice-Hall, 1990.

[5] N. Bhadra, N. Bhadra, K. Kilgore, and K. Gustafson, "High frequency electrical conduction block of pudendal nerve," *J. Neural Eng.*, vol. 3, no. 2, pp. 180–187, Jun. 2006.

[6] N. Bhadra and K. Kilgore, "High-frequency electrical conduction block of mammalian peripheral motor nerve," *Muscle Nerve*, vol. 32, no. 6, pp. 782–790, Dec. 2005.

[7] B. Bowman and D. McNeal, "Response of single alpha motoneurons to high frequency pulse train: Firing behavior and conduction block phenomenon," *Appl. Neurophysiol.*, vol. 49, no. 3, pp. 121–138, 1986.

[8] J. Reboul and A. Rosenblueth, "The action of alternating currents upon the electrical excitability of nerve," *Amer. J. Physiol.*, vol. 125, no. 2, pp. 205–215, Feb. 1939.

[9] A. Rosenblueth and J. Reboul, "The blocking and deblocking effects of alternating currents on nerve," *Amer. J. Physiol.*, vol. 125, pp. 251–264, 1939.

[10] C. Tai, J. Roppolo, and W. de Groat, "Response of external urethral sphincter to high frequency biphasic electrical stimulation of pudendal nerve," *J. Urol.*, vol. 174, no. 2, pp. 782–786, 2005.

[11] J. Tanner, "Reversible blocking of nerve conduction by alternating-current excitation," *Nature*, vol. 195, no. 4842, pp. 712–713, Aug. 1962.

[12] R. Williamson and B. Andrews, "Localized electrical nerve blocking," *IEEE Trans. Biomed. Eng.*, vol. 52, no. 3, pp. 362–370, Mar. 2005.

[13] N. Bhadra, E. Lahowetz, S. Foldes, and K. Kilgore, "Simulation of high-frequency sinusoidal electrical block of mammalian myelinated axons," *J. Comput. Neurosci.*, vol. 22, no. 3, pp. 313–326, Jun. 2007.

[14] C. Tai, W. de Groat, and J. Roppolo, "Simulation analysis of conduction block in unmyelinated axons induced by high-frequency biphasic electrical currents," *IEEE Trans. Biomed. Eng.*, vol. 52, no. 7, pp. 1323–1332, Jul. 2005.

[15] C. Tai, W. de Groat, and J. Roppolo, "Simulation of nerve block by high-frequency sinusoidal electrical current based on the Hodgkin–Huxley model," *IEEE Trans. Neural Syst. Rehabil. Eng.*, vol. 13, no. 3, pp. 415–422, Sep. 2005.

[16] X. Zhang, J. Roppolo, W. de Groat, and C. Tai, "Simulation analysis of conduction block in myelinated axons induced by high-frequency biphasic rectangular pulses," *IEEE Trans. Biomed. Eng.*, vol. 53, no. 7, pp. 1433–1436, Jul. 2006.

[17] X. Zhang, J. Roppolo, W. de Groat, and C. Tai, "Mechanism of nerve conduction block induced by high-frequency biphasic electrical currents," *IEEE Trans. Biomed. Eng.*, vol. 53, no. 12, pp. 2445–2454, Dec. 2006.

[18] J. Wang, B. Shen, J. Roppolo, W. de Groat, and C. Tai, "Influence of frequency and temperature on the mechanisms of nerve conduction block induced by high-frequency biphasic electrical current," *J. Comput. Neurosci.*, vol. 24, pp. 195–206, 2008.

[19] B. Frankenhaeuser and A. Huxley, "The action potential in the myelinated nerve fibre of Xenopus laevis as computed on the basis of voltage clamp data," *J. Physiol.*, vol. 171, no. 2, pp. 302–315, Jun. 1964.

[20] J. Roper and J. Schwarz, "Heterogeneous distribution of fast and slow potassium channels in myelinated rat nerve fibres," *J. Physiol.*, vol. 416, pp. 93–110, Sep. 1989.

[21] J. Schwarz, G. Glassmeier, E. Cooper, T.-C. Kao, H. Nodera, D. Tabuena, R. Kaji, and H. Bostock, "KCNQ channels mediate IKs, a slow K+ current regulating excitability in the rat node of ranvier," *J. Physiol.*, vol. 573, no. 1, pp. 17–34, May 2006.

[22] J. Schwarz, G. Reid, and H. Bostock, "Action potentials and membrane currents in the human node of ranvier," *Pflugers Arch. Eur. J. Physiol.*, vol. 430, no. 2, pp. 283–292, Jun. 1995.

[23] A. Paintal, "The influence of diameter of medullated nerve fibres of cats on the rising and falling phases of the spike and its recovery," *J. Physiol.*, vol. 184, no. 4, pp. 791–811, Jun. 1966.
[24] I. Boyd and K. Kalu, "Scaling factor relating conduction velocity and diameter for myelinated afferent nerve fibres in the cat hind limb," *J. Physiol.*, vol. 289, pp. 277–297, Apr. 1979.
[25] W. Boyce and R. Diprima, *Elementary Differential Equations and Boundary Value Problems*, 6th ed. New York: Wiley, 1997.
[26] F. Rattay, "Analysis of models for external stimulation of axons," *IEEE Trans. Biomed. Eng.*, vol. BME-33, no. 10, pp. 974–977, Oct. 1986.
[27] F. Rattay, "Analysis of models for extracellular fiber stimulation," *IEEE Trans. Biomed. Eng.*, vol. 36, no. 7, pp. 676–682, Jul. 1989.
[28] C. McIntyre, A. Richardson, and W. Grill, "Modeling the excitability of mammalian nerve fibers: Influence of afterpotentials on the recovery cycle," *J. Neurophysiol.*, vol. 87, no. 2, pp. 995–1006, Feb. 2002.
[29] H. Kager, W. Wadman, and G. Somjen, "Simulated seizures and spreading depression in a neuron model incorporating interstitial space and ion concentrations," *J. Neurophysiol.*, vol. 84, no. 1, pp. 495–512, Jul. 2000.
[30] H. Kager, W. Wadman, and G. Somjen, "Conditions for the triggering of spreading depression studied with computer simulations," *J. Neurophysiol.*, vol. 88, no. 5, pp. 2700–2712, Nov. 2002.
[31] M. Bazhenov, I. Timofeev, M. Steriade, and T. Sejnowski, "Potassium model for slow (2–3 Hz) in vivo neocortical paroxysmal oscillations," *J. Neurophysiol.*, vol. 92, no. 2, pp. 1116–1132, Aug. 2004.
[32] M. Bikson, J. Lian, P. Hahn, W. Stacey, C. Sciortino, and D. Durand, "Suppression of epileptiform activity by high frequency sinusoidal fields in rat hippocampal slices," *J. Physiol.*, vol. 531, pp. 181–191, 2001.
[33] J. Lian, M. Bikson, C. Sciortino, W. Stacey, and D. Durand, "Local suppression of epileptiform activity by electrical stimulation in rat hippocampus in vitro," *J. Physiol.*, vol. 547, pp. 427–434, 2003.
[34] A. Jensen and D. Durand, "Suppression of axonal conduction by sinusoidal stimulation in rat hippocampus in vitro," *J. Neural Eng.*, vol. 4, pp. 1–16, 2007.
[35] M. Renganathan, T. Cummins, and S. Waxman, "Contribution of Na_V 1.8 sodium channels to action potential electrogenesis in DRG neurons," *J. Neurophysiol.*, vol. 86, pp. 629–640, 2001.

Hailong Liu was born in Jilin, China, in 1978. He received the B.S. degree in biomedical engineering from the Department of Electrical Engineering, Jilin University, Changchun, China, in 2000, and the Ph.D. degree in biomedical engineering from the Institute of Biomedical Engineering, Xi'an Jiaotong University, Xi'an, China, in 2006.

Since March 2007, he has been a Postdoctoral Fellow in the Department of Pharmacology and the Department of Urology, University of Pittsburgh, Pittsburgh, PA. His current research interests include modeling analysis of nerve response to electrical stimulation, neural control of micturition, brain–computer interface, artificial neural networks, and automatic control.

Dr. Liu is a member of the Society for Neuroscience.

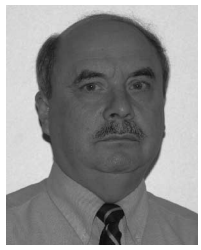

James R. Roppolo received the B.S. degree in pharmacy from the University of Pittsburgh, Pittsburgh, PA, in 1965, and the Ph.D. degree in neuropharmacology from the Department of Pharmacology, University of Michigan School of Medicine, Ann Arbor, in 1970.

He joined as a faculty member in the Department of Pharmacology, University of Pittsburgh School of Medicine, Pittsburgh, where he was engaged in research on neuropharmacology and neurophysiology, and is currently an Assistant Professor. His current research interests include central antonomic pathways that control bladder, colon, and sexual functions, as well as the somatic motor pathways that produce limb movements, and the restoration of autonomic and motor function following spinal cord injury.

Dr. Roppolo is a member of the Society for Neuroscience.

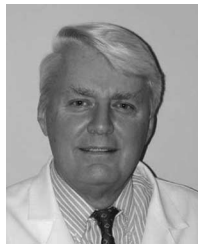

William C. de Groat received the B.S. degree in pharmacy and the M.S. degree from Philadelphia College of Pharmacy and Sciences, Philadelphia, PA, in 1960 and 1962, respectively, and the Ph.D. degree in pharmacology from the Department of Pharmacology, University of Pennsylvania Medical School, Philadelphia, in 1965.

He was engaged in research on neurophysiology in the Department of Physiology, John Curtin School of Medical Research, Canberra, A.C.T., Australia. In 1968, he joined the Department of Pharmacology, University of Pittsburgh School of Medicine, Pittsburgh, PA, where he is currently a Professor of pharmacology. His laboratory is studying the organization of the lumbosacral autonomic reflex pathways in a variety of animal models. His current research interests include identity of the neurotransmitters at peripheral ganglionic and central autonomic synapses, the central mechanisms involved in viscerosomatic integration, the maturation of autonomic reflexes during postnatal development, the mechanisms underlying the recovery of function following spinal cord injury, and visceral nociceptive pathways.

Changfeng Tai (M'97–SM'01) received the B.S., M.S., and Ph.D. degrees in biomedical engineering from Xi'an Jiaotong University, Xi'an, China, in 1986, 1989, and 1992, respectively.

He was with the Department of Rehabilitation Science and Technology, University of Pittsburgh, Pittsburgh, PA, where he joined the Department of Pharmacology as a faculty member, and is currently an Assistant Professor in the Department of Urology. His current research interests include functional neuromuscular stimulation to restore micturiton and locomotion functions after spinal cord injury, model analysis of nerve stimulation, biomedical signal processing, and neural control of micturition.

Dr. Tai is a member of the Society for Neuroscience.